Chapter 6: Matching ocular biometry to optical aberrations: Chick and mouse computer eye models

Resumen capítulo 6:

Relación de la biometría ocular con las aberraciones ópticas: modelos de ojo de pollo y ratón.

En este capítulo hemos desarrollado un modelo de ojo de pollo (de 0 a 14 días) y un modelo de ojo de ratón de 4 semanas de edad. Estos modelos computacionales están basados en datos biométricos obtenidos de la literatura y en las medidas realizas en ambos animales en estudios previos, descritos en capítulos anteriores de esta tesis.

Las aberraciones oculares han sido reproducidas utilizando técnicas de trazado de rayos para cada modelo de ojo y comparado posteriormente con las medidas realizadas con aberrometría. Esta comparación ha permitido evaluar la precisión de los datos biométricos en dichos modelos animales y predecir el papel de algunas estructuras oculars, de las que hasta el momento se conoce poco en estos ojos, como la distribución de índice refractivo del cristalino o posibles asfericidades.

En pollos, encontramos que las variaciones de los radios de curvatura corneales, espesor corneal, profundidad de cámara anterior, radios de curvatura y espesor del cristalino, así como la longitud axial, por sí solos no pueden explicar los cambios longitudinales con la edad de la refracción y las aberraciones ópticas medidas experimentalmente. El modelo predice el papel que juega la distribución de gradiente de índice para explicar las magnitudes observadas y los cambios de desenfoque y aberración esférica. Además también demuestra la fiabilidad de los diferentes parámetros oculares obtenidos de la literatura, a veces controvertidos.

Las diferencias de refracción y aberraciones ópticas entre ojos miopes y emmetropes pueden ser explicados por razones principalmente relacionadas con la elongación axial ocular.

En el ratón, la degradación de la óptica del ojo (ver capítulo 5) abre la pregunta sobre el papel que desempeñan las distintas estructuras en la calidad de la imagen retiniana. Los datos biométricos publicados de ratones de 4 semanas de edad (radios de curvatura, espesores...) no explican, al igual que en el pollo, los valores de desenfoque y aberraciones obtenidos experimentalmente. Se hace necesario estudiar por métodos computacionales el posible papel de la distribución del gradiente de índice del cristalino.

This chapter is based on the articles by García de la Cera et al.:

"Matching ocular biometry to optical aberrations (I): Developing normal and myopic chick computer eye model", in preparation.

"Matching ocular biometry to optical aberrations (II): 4-week old mouse computer eye model", in preparation.

The contribution of Elena García de la Cera to the study was the literature search and analysis of ocular biometry data, measurement of ocular biometry and optical aberrations in the mouse and chick, development of the computer eye models and data analysis.

Coauthors of the study are Alberto de Castro, Sergio Barbero and Susana Marcos.

6.1. Abstract

In this chapter we have developed a chick eye computer model from 0 to 14 days of age and a 4 week-old mouse eye computer model based on biometric data from the literature and from previous chapters in this thesis. Ocular aberrations have been simulated using ray tracing on these models and compared to the experimental aberrometry measurements presented in this thesis. This comparison has allowed us to evaluate the accuracy of biometric data in these animal models and predict the role of some ocular parameters from which little is known in these eyes (i.e. refractive index distribution or surface asphericities)

In chicks, we found that changes in corneal radii of curvature, corneal thickness, anterior chamber depth, lens radii of curvature and thickness, and axial length alone could not explain the longitudinal changes in refraction and optical aberrations measured in chicks. The model predicts a prominent role of gradient index distribution to explain the observed amounts and changes of defocus and spherical aberration. The model also tests the plausibility of the different ocular biometry data (sometimes controversial) from the literature. Differences in refraction and optical aberrations between normal and myopic eyes can be explained primarily by simple ocular axial elongation

The severely degraded optics in mice eye (see Chapter 5) can be explained by the geometrical structure of the ocular components (radii of curvature, corneal thickness, anterior chamber depth, lens radii of curvature and thickness, and axial length). A model with a homogeneous index of refraction in the lens would predict even larger amounts of aberrations.. A plausible gradient index profile in the lens was assumed, and allowed to reproduce experimental data.

6.2. Introduction

Ocular biometry in animal models of myopia has been widely reported, as it is critical to assess the structural changes of the ocular components during development of the normal eye, or the eye undergoing treatments leading to refractive errors. More recently, aberrometers have been developed that have allowed for the first time the measurement of optical aberrations in animal eyes (chicks (García de la Cera et al. 2006; Kisilak et al. 2006; Tian and Wildsoet 2006; García de la Cera et al. 2007), mice (García de la Cera et al. 2006) -presented in this thesis-, cat (Huxlin et al. 2004)or monkeys (Ramamirtham et al. 2006). Aberrations have been measured both in wild type species and normal eyes, during normal development and during development of refractive errors (imposed by form deprivation or lenses), as presented in this thesis.

The geometrical and structural properties of the ocular components are intrinsically related to the optical quality of the eye. Schematic eye models in the chick (Schaeffel and Howland 1988) , mouse (Remtulla and Hallett 1985), rat (Hughes 1979) or primate (Lapuerta and Schein 1995) eyes have been reported in the literature, similarly to well-known schematic model eyes of the human. However, in most cases, these models have been used to predict paraxial properties of the eye, most frequently refractive errors. Today, customized computer eye models of the human eye, primarily pseudophakic eyes have been shown to predict experimentally measured high order aberrations with a high accuracy (Rosales and Marcos 2007). These model eyes include individual data of corneal topography, lens geometry and misalignments, and the off-axis location of the fovea (Rosales and Marcos 2006). Also, the use of schematic model eyes is important to assess the relative importance of each component to the overall optical quality, and to identify the potential contribution of unknown factors (such as the refractive index of the lens, or asphericities). Also, while previous simulations of optical quality with increasing age have been able to extract suggestive suggestions (such as the geometrical nature of the improvement of optical quality in chicks, for constant pupil sizes), those were

based on very simple models (Howland 2005). Schematic models including all known parameters will provide more extended predictability.

In this chapter we developed computer models of chick and mice eyes to understand the sources of optical degradation in these eyes. We used refraction and ocular biometry data obtained both in this thesis as well as in previous studies in the literature and developed schematic eye models to predict high order ocular aberrations (primarily spherical aberration). The simulated aberrations were compared to measured aberrations (reported in this thesis). We will assess the impact of the change of the ocular components with development and across refractive errors on the optical aberrations, to which extent geometrical and structural properties of the ocular components, and the potential role of not well known properties (gradient index, surface asphericities).

This chapter presents a comprehensive review of ocular parameters of the chick eye of different ages (Section 6.3.1), sometimes controversial across studies. The most plausible data geometrical and structural properties of the cornea, crystalline lens and interocular distances have been identified, to explain the changes in refraction and spherical aberration with age and refractive errors. .

6.2.1. A compilation of chick biometric data

Biometric data have been compiled from various sources. Data include anterior corneal radius and asphericity, corneal thickness, anterior chamber depth, lens radii of curvature, refractive indices, lens thickness and axial length. Table 6.1 (A & B) summarizes the data from the different studies that we have tested in the reported model eyes and used to simulate the optical aberration. Figures 6.1-6.7 show the change of ocular biometry parameters in the chick eye as a function of age, from different studies.

Ocular parameter	Reference	Total number of eyes	Age range (days)	Longitudinal study	Experimental condition	Technic used
Anterior Corneal radius	Gottlieb et al.,1987		0-44	yes	in vivo	keratometry
	Li et al., 2000	10	0-15	yes	in vivo	photokeratometry
	Wallman & Adams, 1987	10	0-17	yes	in vivo	photokeratometry
	Troilo et al.1987	12	0-30	yes	anaesthetized	keratometry
	Li & Howland,2003	12	21	no	in vivo	photokeratometry
	García de la Cera et al., 2007	10	0-13	Yes	in vivo	photokeratometry
	Guggenheim et al., 2002	10	28	no	anaesthetized	keratometry
	Troilo & Wallman, 1991	9	14	no	anaesthetized	keratometry
	Troilo & Wallman, 1987		28	no	anaesthetized	keratometry
	Schaeffel & Howland, 1988	156	14-86		in vivo	photokeratometry
	Irving et.al,1996	234	0-14	Yes	in vivo	keratometry
Corneal asphericity	Schaeffel & Howland, 1987	4	14-42		in vivo	photokeratometry
Corneal thickness	Montiani-Ferrerira, 2004	25	0-450	yes	in vivo	Ultrasonic pachimetry
	Irving et.al,1996	234	0-14	yes	ex vivo	
	Irving et.al,1996	52	14		ex vivo	measurements of frozen sections
	Choh & Sivak,2002 (a)	9	7	no	ex vivo	ultrasound biomicroscopy
n corneal	Sivak & Mandelman,1982	4		no	ex vivo	refractometry
	Irving et.al,1996	6	Adults		ex vivo	Abbe-refractometry
Anterior chamber	Gottlieb et al.,1987		0-43	yes	in vivo	A-scan ultrasonography
	Li et al., 2000	10	0-14	yes	in vivo	A-scan ultrasonography
	Wallman et al.,1994	16	12,32	no	in vivo	Ultrasonography
	Zhu et al.,1995	103	14,28	no	anaesthetized	A-scan ultrasonography
	Guggenheim et al., 2002	10	28	no	anaesthetized	A-scan ultrasonography
	Li & Howland,2003	12	21	no	in vivo	A-scan ultrasonography
	Troilo & Wallman, 1991	9	14	no	anaesthetized	A-scan ultrasonography
	Pickett-Seltner et al.,1988	10	0-15	Yes	ex vivo	measurements of frozen sections
	Schaeffel & Howland, 1988	20	30		ex vivo	measurements of frozen sections
	Irving et.al,1996	234	0-14	yes	ex vivo	A-scan ultrasonography
	Irving et.al,1996	52	14		ex vivo	measurements of frozen sections
	Choh et al,2002 (a)	9	7	no	ex vivo	ultrasound biomicroscopy
n humors	Irving et.al,1996	6	Adults		ex vivo	Abbe-refractometry

Table 6.1 (A). A compilation of cornea and anterior chamber biometric data used in this work. Empty cells are data that are not indicated by authors. Posterior corneal radius is not show because they are not real measurements but estimations.

Ocular parameter	Reference	Total number of eyes	Age range days)	Longitudinal study	Experimental condition	Technic used
Anterior lens radius	Irving et.al,1996	52	14		ex vivo	measurements of frozen sections
	Schaeffel & Howland, 1988	20	30		ex vivo	measurements of frozen sections
Lens thickness	Gottlieb et al.,1987		0-45	yes	in vivo	A-scan ultrasonography
	Troilo et al.1987	12	0-29	yes	anaesthetized	A-scan ultrasonography
	Nickla et al.1997	10	1,5	no	anaesthetized	A-scan ultrasonography
	Zhu et al.,1995	103	14,28	no	anaesthetized	A-scan ultrasonography
	Guggenheim et al., 2002	10	28	no	anaesthetized	A-scan ultrasonography
	Priolo et al.,1999	15	0,7	no	ex vivo	Vernier calipers
	Priolo et al.,2000	12	0,7	no	in vivo	Scanning electron microscopy
	Troilo & Wallman, 1991		21			Vernier calipers
	Schaeffel & Howland, 1988	20	30		anaesthetized	Ultrasound
	Irving et.al,1996	234	0-14	yes	ex vivo	A-scan ultrasonography
	Irving et.al,1996	52	14		ex vivo	measurements of frozen sections
	Choh & Sivak,2002 (a)	12	8	no	ex vivo	ultrasound biomicroscopy
n lens	Sivak & Mandelman,1982	4		no	ex vivo	spectometry
	Schaeffel & Howland, 1988	156	14-86	Yes	ex vivo	refractometry
Posterior radius lens	Irving et.al,1996	52	14		ex vivo	measurements of frozen sections
	Wallman & Adams, 1987	10	0-18	yes	in vivo	Purkinje image photography
	Sivak et al,1978		20-55	no	ex vivo	refractometry
n posterior chamber depth	Sivak & Mandelman,1982	2		no	ex vivo	refractometry
Axial length	Pickett-Seltner et al.,1988	10	0-14	Yes	ex vivo	measurements of frozen sections
	Schaeffel & Howland, 1988	38	14-86		ex vivo	photography of transscleral images
	Irving et.al,1996	234	0-14	yes	ex vivo	A-scan ultrasonography
	Irving et.al,1996	52	14		ex vivo	measurements of frozen sections
	Choh & Sivak,2002 (a)	12	7	no	ex vivo	A-scan ultrasonography
	Gottlieb et al.,1987		0-42	yes	in vivo	A-scan ultrasonography/ measurements of frozen sections
	Zhu et al.,1995	103	14,28	no	anaesthetized	A-scan ultrasonography
	Pickett-Seltner et al.,1987	10	0,14	no	ex vivo	Vernier calipers
	García de la Cera et al., 2006	10	0-13	Yes	in vivo	A-scan ultrasonography

Table 6.1 (B). A compilation of lens, posterior chamber depth and axial length biometric data used in this work. Empty cells are data no indicated by authors.

6.2.1.1. Anterior corneal radius

The cornea is the most important refractive surface in the eye, and corneal curvature is an important contributor to the refractive state. Most data in the literature report anterior corneal radius for chicks of 2-weeks (see Figure 6.1) (Gottlieb et al. 1987; Troilo et al. 1987; Wallman and Adams 1987; Troilo and Wallman 1991; Li et al. 2000; Guggenheim et al. 2002; García de la Cera et al. 2007) and 4-weeks of age (Gottlieb et al. 1987; Troilo et al. 1987; Wallman and Adams 1987; Troilo and Wallman 1991; Guggenheim et al. 2002). Fewer studies report data for 1-week old chicks (Wallman and Adams 1987; Choh and Sivak 2005). Irving et al. (Irving et al. 1996) and Schaeffel & Wallman (Schaeffel and Howland 1988) proposed empirical equations for the change of the anterior corneal radius, although not all reported data in the literature match those equations. Irving et al's data differ the most from other studies, as they report that corneal radius of curvature is constant for the first four days and then increases linearly at rate of 0.05mm/day. However, the behavior is probably not well described by a linear fit. In general, the values reported by Irving et al are higher than other data in the literature, especially for older chicks (see Table 6.1). On the other hand, Schaeffel & Howland (1988) model fits accurately the data from most studies, especially in the second week of age (9-16 days in the data from our own lab) and agree with our data in that period, but diverge from several of the reported data in the first week of age (Wallman and Adams 1987; Choh and Sivak 2005).

While most studies only report corneal radius of curvature, there is evidence that the chick cornea may be an aspheric surface. Corneal asphericity on the pupillary area (Schaeffel and Howland 1987) may have a role in the total spherical aberration of the chick eye. We incorporated corneal asphericity in the model, based on Schaeffel & Howland (Schaeffel and Howland 1987) measurements on corneal radius of curvature at two different corneal areas: corneal center and 1.7 mm off-axis, on two 42-days old chicks. However, the results reported in this study on two different

chicks are not conclusive. One chick showed no change of radius of curvature from the center to the periphery, while the other showed a radius of 3.95 mm at the corneal center and 4.08 mm off-axis. Using the definition of a conic surface (Atchison and Smith 2000), these values are consistent with an asphericity of -1.12, which would yield a negative corneal spherical aberration in the cornea (opposite to the human cornea, which is flatter in the center than in the periphery, with an average asphericity of –0.26, and generally positive spherical aberration) (Atchison and Smith 2000). As we will discuss later, this hyperboloid corneal shape does not appear to be consistent with the measured spherical aberration and plausible structure of the crystalline lens, at least in the range period of 0-14 day-old chicks, and therefore other values of asphericity will be also tested.

Corneal radii have been reported in ammetropic chick eyes. High levels of hyperopia are associated with corneal flattening (Irving et al. 1992)and form-deprived myopic eyes with steeper corneas (Gottlieb et al. 1987). In our model we have considered myopic eyes with (1) a simple

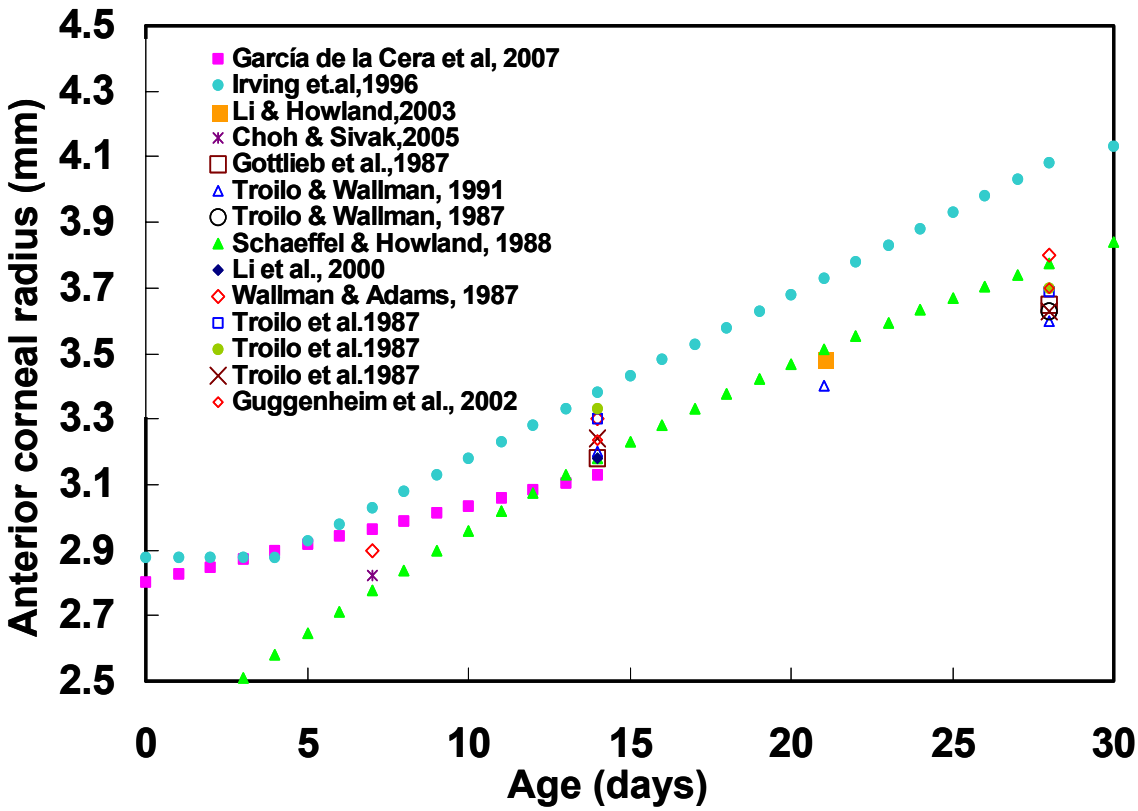

Figure 6.1 Anterior corneal radius reported values from several authors.

elongation of the posterior chamber (2) other ocular changes reported in myopic eyes (Gottlieb et al. 1987; Schaeffel and Howland 1988; Irving et al. 1992).

6.2.1.2. Corneal thickness

Irving et al. (Irving et al. 1996) proposed a constant corneal thickness over the first 14 days of life. On the other hand, Montiani-Ferreira et al.(Montiani-Ferreira et al. 2004) measured variations in the central corneal thickness due to maturation of corneal endothelial cell function until 70 days of age (0.247 mm), when corneal maturity is reached. This study reports a decrease of the central corneal thickness from hatching (0.242 mm) until 12 days of age, when a minimum value was measured (0.238 mm), an then it gradually increased. This trend has also been reported in dogs (Montiani-Ferreira et al. 2003) and human (Portellinha and Belfort 1991). Schaeffel (Schaeffel and Howland 1988)reported similar corneal thickness in 30-day old chicks (0.24 mm) and Hayes et al (Hayes et al. 1986) reported 0.26 mm,

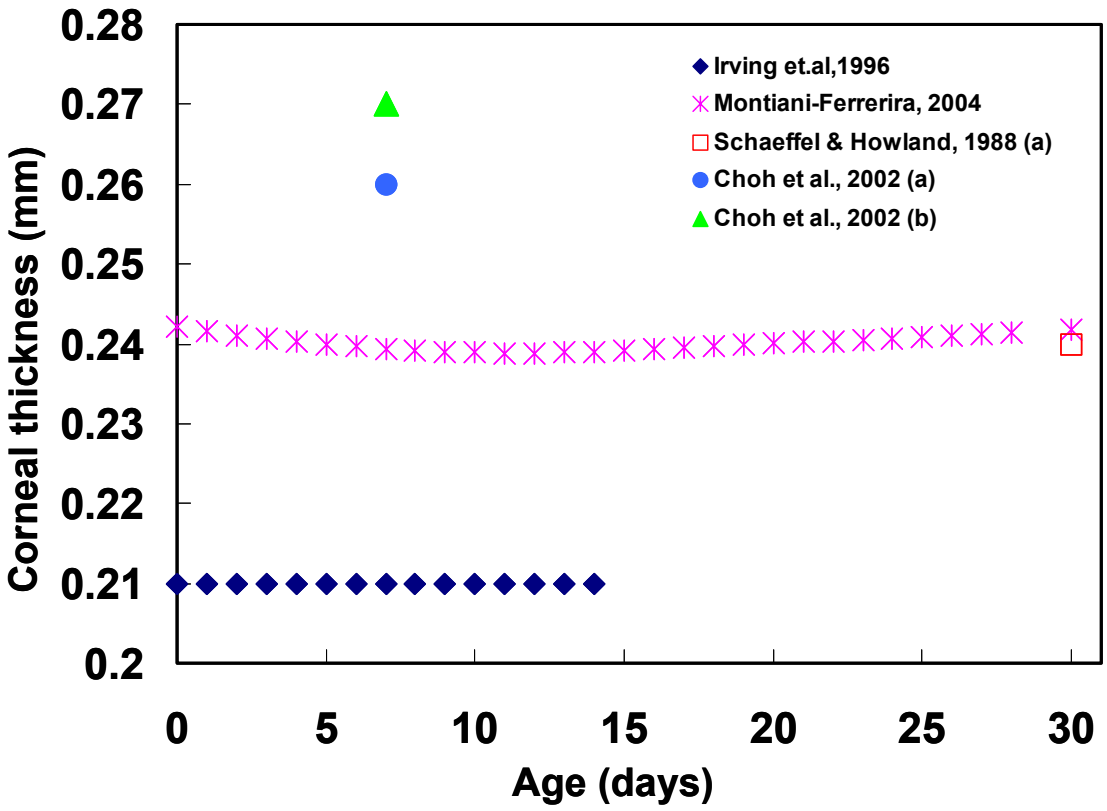

Figure 6.2 Corneal thickness from several authors.

on average for 22 to 55 days old chicks. Choh et. al 2002 (Choh et al. 2002) reported slightly higher values than other studies (0.26 -0.27 mm) in 7-day old chicks. We used the expression proposed by Montiani-Ferreira et al. (Montiani-Ferreira et al. 2004) for the change of corneal thickness with age in the range of ages of our study. Figure 6.2 shows central corneal thickness from several studies and Irving and Howland prediction models.

6.2.1.3. Posterior corneal radius

Posterior corneal surface measurements are technically more challenging than the anterior corneal ones, and to our knowledge, only two studies have attempted the estimation of the posterior corneal radius in chicks from refractive index and power measurements in ex vivo corneas. Choh & Sivak (Choh and Sivak 2005) estimated posterior corneal radius of 2.53 mm for 7-day old chicks (lower than anterior corneal radius, 2.82 mm) from Schaeffel & Howland anterior radius predictions(Schaeffel and Howland 1988). Schaeffel & Howland (1988) used the same corneal radius for the anterior and posterior surface (3.84 mm) in their 30-day old chick schematic eye model.

In human there is a correlation between anterior and posterior corneal radius, with the posterior radius of curvature 0.81 times the anterior radius (Atchison and Smith 2000). Since longitudinal data of posterior corneal radius are not available, we assumed similar values and change rate for the anterior and posterior corneal radii, as previously done by Schaeffel & Howland (1988). We tested that slight variations of the corneal posterior surface do not produce significant changes in the total defocus and aberrations of the eye.

6.2.1.4. Corneal index of refraction

Sivak & Mandelman,1982 proposed a corneal refractive index of 1.369 and Choh & Sivak (Choh and Sivak 2005) an index of 1.373, similar

than reported by Schaeffel & Howland (1988). These are average data, as the cornea is actually a multilayer structure (Barbero 2006). We used the more recent value from Choh & Sivak (2005). The index of refraction of the chick cornea appears to be lower than the mean index of refraction of the human cornea, 1.376 (Atchison and Smith 2000).

6.2.1.5. Anterior chamber depth

In humans and primates, anterior chamber depth increases during the first years of development (until two years of age in infants, (Curtin 1985) and until at least 1 year in marmosets (Troilo and Judge 1993).

The anterior chamber depth in chicks has been widely reported in the literature (and results are summarized in Figure 6.3). Irving et al. (Irving et al. 1996) showed lower anterior chamber depth values than most authors (although they showed higher axial lengths). Troilo & Wallman's data on 7-

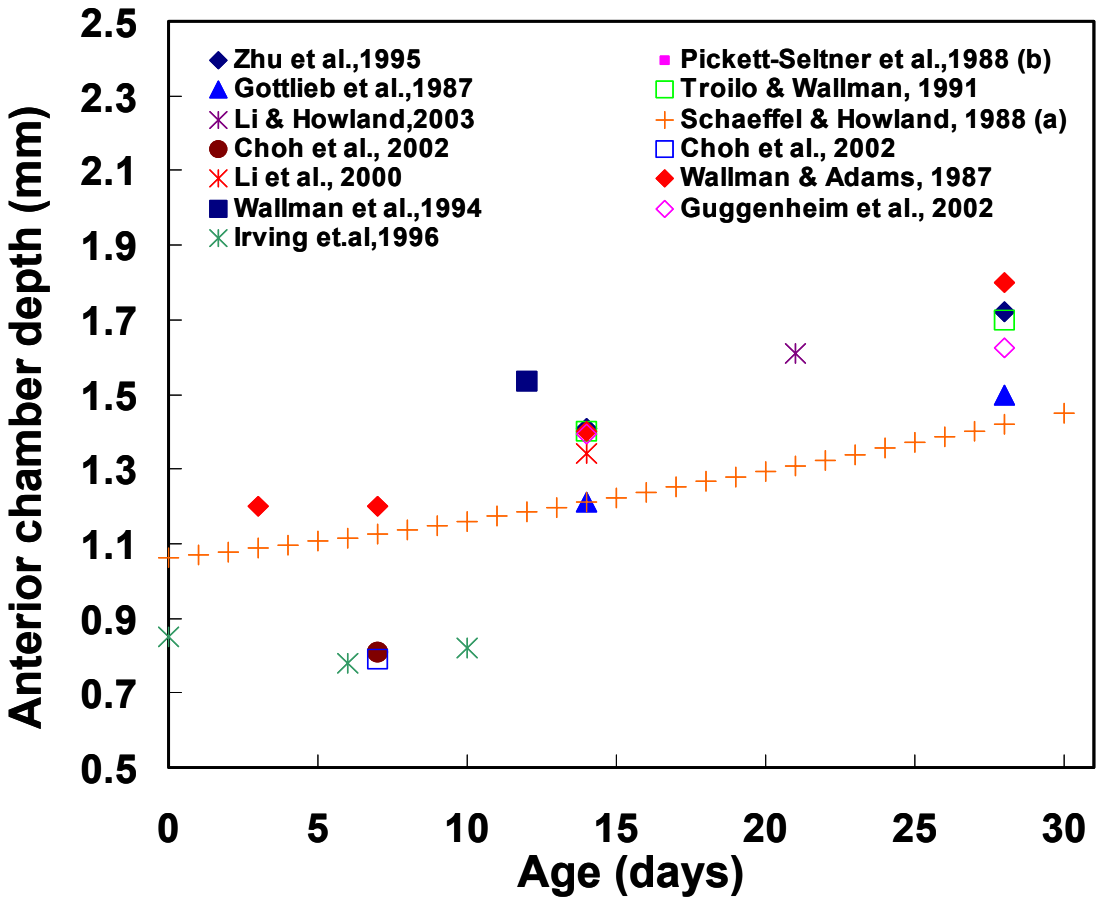

Figure 6.3 Anterior chamber depth reported values from several authors.

day old chicks appear also above average. We used an empirical expression for the change of anterior chamber depth with age obtained from average results (Schaeffel and Howland 1988). The aqueous index of refraction was measured in vitro by Schaeffel and Howland (1988) by an Abbe refractometer, and it is similar than vitreous chamber n=1.335 (Schaeffel and Howland 1988)

Form deprived eyes have deeper anterior chamber depths relative to normal eyes and this increase has been reported to be proportional to total axial length (Gottlieb et al. 1987).

6.2.1.6. *Anterior lens radius*

Lens parameters are not easily accessible, as phakometry techniques used in humans (Mutti et al. 1992; Rosales and Marcos 2006; Rosales and Marcos 2007) do not appear to have been much used in the chick, they have been used however in other animal models such as Rhesus Monkeys. Changes in crystalline lens radii of curvature and lens tilt and decentration during dynamic accommodation in Rhesus Monkeys (Rosales et al. 2008). Other optical properties of the lens, such as a possible gradient refractive index have little been addressed in vitro, and never been measured in vivo. Some studies suggest no or little changes in focal length of the chick crystalline lens (Pickett-Seltner et al. 1988; Sivak et al. 1989) with development, and also with treatments. These authors argue that lens is a “genetically preprogrammed feature” and not easily influenced by environment. However, other authors found changes in lens size and shape from frozen sections, and most models in the literature assume crystalline lens radius of curvature that increase linearly with age, at various rates ranging from 0.11 mm/day from Irving et al. (Irving et al. 1996) to 0.04 mm/day Schaeffel & Wallman (Schaeffel and Howland 1988). Figure 6.4 shows a plot of the anterior lens radius as a function of age from several studies. In the human eye, the lens surfaces have been described using conical surfaces (Dubbelman and Van der Heijde 2004). No data on the asphericity of the chick lens surfaces has been reported.

Several studies have measured the spherical aberration of isolated chick lenses. In lenses from hatchling chicks, spherical aberration varied non-monotonically between positive and negative, with an overall negative spherical aberration predominating (Choh et al. 2002). A study by (Sivak et al. 1989) showed that lens spherical aberration does not increase with development. It should be noted that typically, laser ray tracing techniques used on isolated lenses deliver parallel rays of light (and do not mimic the physiological condition), and therefore the measured spherical aberration cannot be directly compared to that of the cornea. Also, the state of accommodation of isolated human lenses is not necessarily relaxed.

Several studies (Hayes et al. 1986; Pickettseltner et al. 1987) report that there is no change in the chick lens morphology (size, shape, soluble protein content, focal length and transmittance) after induction of myopia.

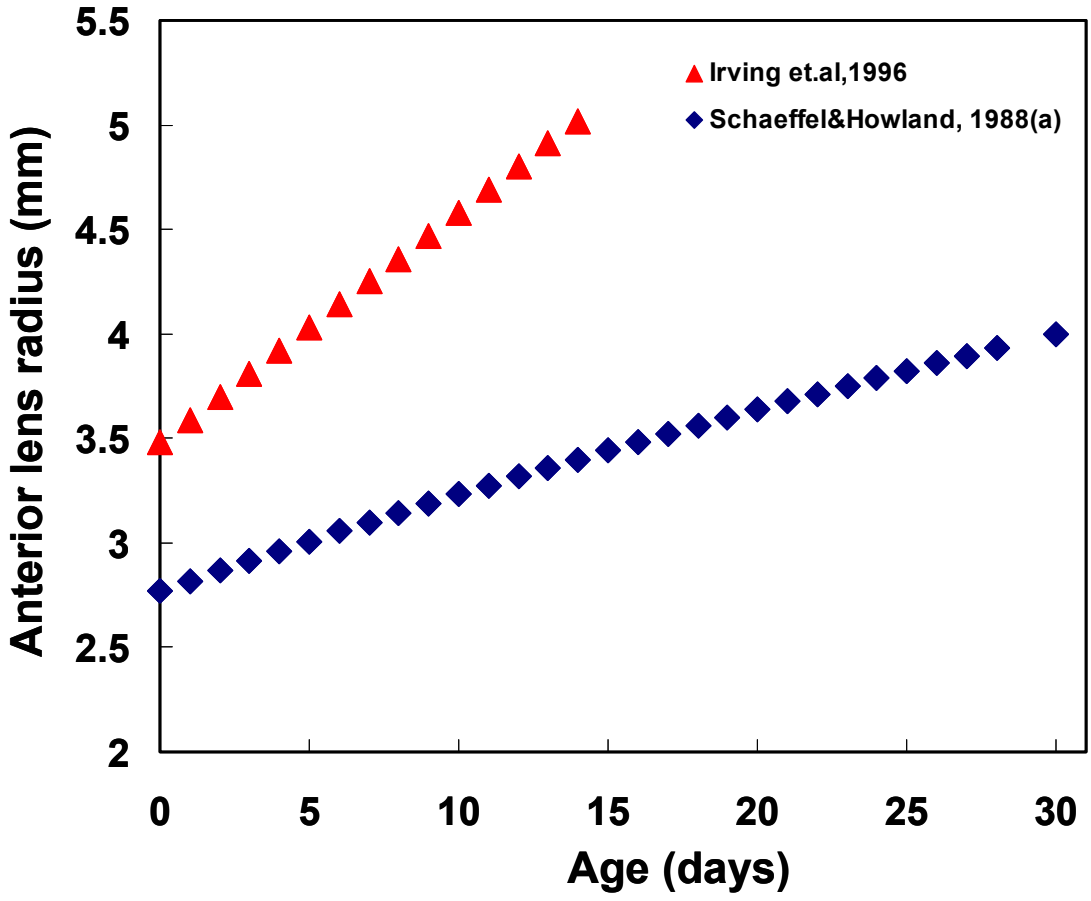

Figure 6.4 Anterior lens radius reported values from several authors.

6.2.1.7. Lens thickness

Figure 6.5 compares measurements of lens thickness as a function age from various studies. Most data, except for those by Irving et al. (Irving et al. 1992) are within close agreement. Lens thickness seems to increase slightly during development. Data from younger chicks appear more variable. The model proposed by Schaeffel and Howland (Schaeffel and Howland 1988) appears to fit most data and was used in our model.

Also, lens thickness in the chick seems to be similar in normal and ametropic eyes. Irving et al. (Irving et al. 1992) observed no differences in lens thickness between control and goggled eyes in myopic or hyperopic chicks induced by goggles from -20 D to +30 D. Gottlieb et al reported the same effect in visually deprived chicks (Gottlieb et al. 1987).

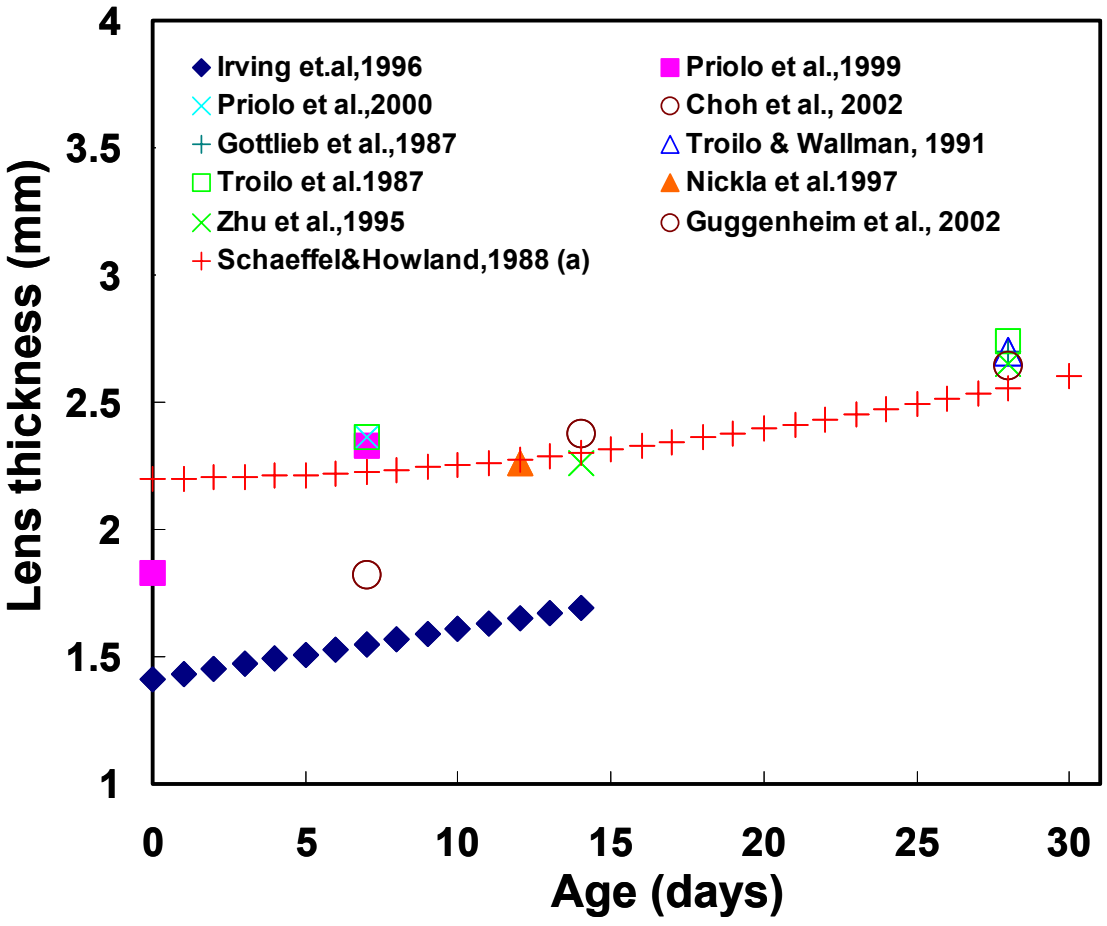

Figure 6.5 Lens thickness reported values from several authors.

6.2.1.8. Lens index refraction of refraction

Very little is known about the refractive index of the lens. Analysis of fiber cell growth in the developing chicken lens (Bassnett and Winzenburger 2003), has led to suggest that the chick lens exhibits a gradient index profile due to the higher concentration of cytoplasmic protein in cells in the center of the lens, and this is likely to change with age, although studies on the potential gradient index profile in the chick lens have never been presented. The Abbe refractometer technique (Sivak and Mandelman 1982), useful for other optical structures index measurements, is not for the complex index gradient from squeezed lens. For an adult chick lens Sivak & Mandelman,1982 (Sivak and Mandelman 1982), estimated an index of 1.3738 in the lens periphery and 1.3947 in the lens core. Schaeffel & Howland assumed an equivalent refractive index of 1.455 to mach the observed refractive state. In humans the reported equivalent refractive index of the unaccommodated eye is 1.42 (Atchison and Smith 2000) . We have implemented in our computer chick model both a crystalline lens with a constant refractive index and a parabolic index profile, monotonically decreasing from the center to the periphery according the values reported by Sivak and Mandelmann.

Priolo et al. (Priolo et al. 2000) attributed to changes in the refractive index distribution the differences in the focal length observed in the lens between form-deprived myopic chicks and normal eyes, while the lens shapes appeared unchanged. However, Pickett-Seltner et al. (Pickettseltner et al. 1987) did not observe changes in the lens focal length, light transmittance or protein content in myopic chick eyes with respect to normal eyes.

Index refractive values of all eye components were maintained constant for this period of time. The refractive index of the lens has been described as a gradient function. We used a spherical gradient profile, with spherical symmetry given by equation:

$n(r) = n_0 \alpha(r- R)+\beta (r-R)^2$ (eq. 6.1)

where R is the half of the lens thickness and α, β are fitting variables (that are varied to match experimental values of spherical aberration). Parabollic gradient index lens functions have been extensively used in human (Blaker 1980); (Nakao et al. 1963) rabbit (Nakao et al. 1968) or cat (Jagger 1990), although higher order quadratic functions have been proposed in the human (Pierscionek and Chan 1989) or fish (Garner et al. 2001). For a review see (Smith 2003).

In our model, we assumed changes with age in the gradient refractive index of the lens, particularly an increase in the index of the periphery, while the core index remains constant, which seems to be anatomically plausible.

6.2.1.9. Posterior lens radius

Measurements of the posterior lens radius of curvature are scarce. The increase of posterior radius with age suggested by (Irving et al. 1996), from 1.97 mm (day 0) to 2.69 mm (day 14) seems higher than the data by

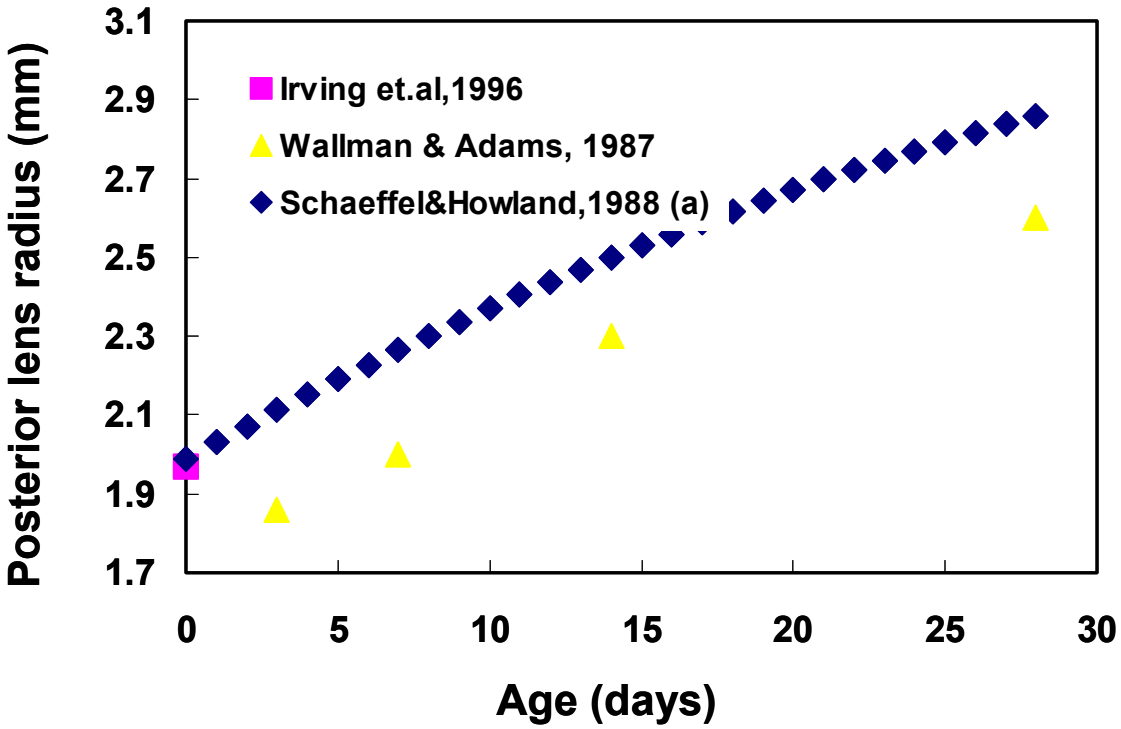

Figure 6.6 Posterior lens radius reported values from several authors.

Wallman & Adams 1987 (Wallman and Adams 1987)or the data used by Schaeffel and Howland, 1988 (Schaeffel and Howland 1988) in their model. Figure 6.6 shows posterior lens radius of curvature from different authors. We choose the values from (Schaeffel and Howland 1988) in our model.

6.2.1.10. Posterior chamber & axial length

Figure 6.7 shows axial length from different studies, including data reported in Chapter 3 of this thesis (which were used in the chick eye computer model) (Gottlieb et al. 1987; Pickettseltner et al. 1987; Pickett-Seltner et al. 1988; Schaeffel et al. 1988; Schaeffel and Howland 1988; Zhu et al. 1995; Irving et al. 1996; Guggenheim et al. 2002; Choh and Sivak 2005; García de la Cera et al. 2006; García de la Cera et al. 2007) . Data are very close although, differences seem to be higher for older chicks. The axial length data measured in this thesis (Chapter 3) agree well with those found in the literature during the first two weeks of age, although these

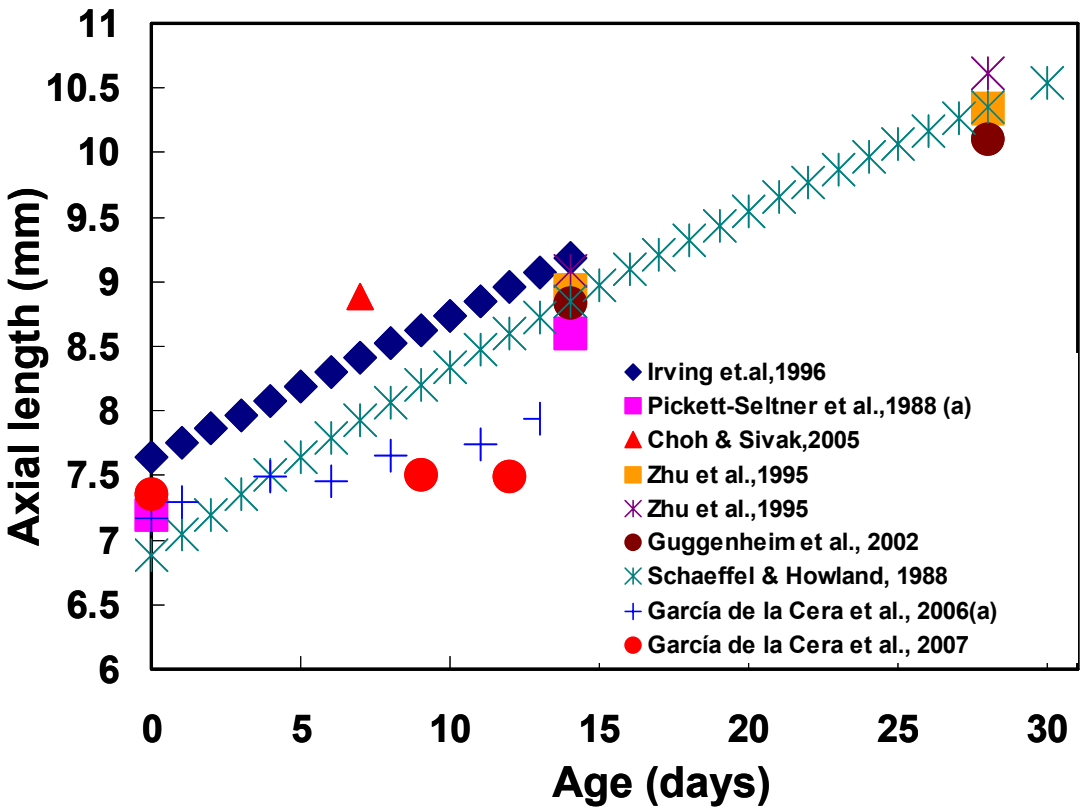

Figure 6.7 Axial length reported values from several authors.

measurements could not be extrapolated with in older chicks. We used data from the lineal regression from our experimental values explained in Chapter 3 for the change in axial length with age.

Posterior chamber depth was estimated as the difference of axial length minus corneal thickness, anterior chamber depth and lens thickness, no constant with age.

To model myopic chick eyes, we used the linear regression of axial length (and posterior chamber depth) of form-deprived eyes to data of Figure 3.2 (A) in Chapter 3. This parameter represents the major difference between the normal and myopic chick eye (Wallman and Adams 1987; Schaeffel and Howland 1991; Kee et al. 2001; Winawer and Wallman 2002).

To our knowledge the only data reported for vitreous chamber refractive index is that of (Sivak and Mandelman 1982), Sivak & Mandelmann (n= 1.3352).

6.2.2. A compilation of mice biometric data

Biometric data have been compiled from various sources. Despite the interest in the mouse as an experimental model of myopia and ocular disease, data are not so extensive as in the chick eye. Data compiled from the different studies are shown in Table 6.2. As in the chick model, we have tested this data in a computer model eye, which has been then used to simulate refractive state and the optical aberrations measured with a Hartmann-Shack aberrometer in a 4 week-year old wild type mice (García de la Cera et al. 2006) (experimental data presented in Chapter 5).

Corneal thickness, anterior chamber depth, lens thickens and posterior chamber depth change with age. The longitudinal changes of these parameters are reported by Schmucker & Schaeffel (Schmucker and Schaeffel 2004) that report a linear increase with age, and we used these expressions for 4-weeks of age.

Schmucker & Schaeffel reported in vivo measurements of the anterior corneal radius with a photekeratometic technique and also ex vivo measurements from frozen sections. More recent biometric data were obtained by Schmucker & Schaeffel (Schmucker and Schaeffel 2004)using Optical Low Coherence Interferometry) and we used those in our model. There is also some evidences that the mouse cornea may be an aspheric surface (Remtulla and Hallett 1985; Schmucker and Schaeffel 2004).

The lens in the mouse has a higher optical relevance than in other species, as it accounts 56% of the optical pathway in the eye. Radii of the lens were reported by Schmucker & Schaeffel, 2004 (Schmucker and Schaeffel 2004) calculated from photography of frozen sections. The lens was considered as a gradient index structure, spherical model, which follows the expression (eq 6.1).

Schmucker & Schaeffel (Schmucker and Schaeffel 2004) estimated an equivalent refractive index which increases with age. Retmulla & Hallett (Remtulla and Hallett 1985) reported similar value that Schmucker & Schaeffel predictions for adult mice.

Axial length measurements with conventional methods such as A-scan ultrasonography are challenging due to small ocular dimensions. Measurement errors have been reported to be of the same order or greater than axial differences resulting from treatments to induce myopia. Much higher accuracy and reproducibility has been achieved using optical low coherence interferometry. Reported axial length at birth in mice is 1.32 mm of axial length, and achieves 90 % of the total size at 100 days (Schmucker and Schaeffel 2004) (3.15 mm at 4-weeks).

Ocular parameter	Reference	Total number of eyes	Age range (days)	Experimental condition	Technic used	Data measured
Anterior Cornea radius	Schmucker & Schaeffel, 2004	11	35,58,75	anesthetized	Photokeratometry	1,49194 (4 week) *
	Schmucker & Schaeffel, 2004		22-100	ex vivo	Photography from frozen	1,41194 (4 week)
Corneal thickness	Schuliz (2003)	8	4 months	in vivo	OLCR (Optical low coherence reflectomety)	0,106mm (4 month)
	Schmucker & Schaeffel, 2004		4week		OLCI (Optical low coherence reflectomety)	0,085 (4 week)*
	Schmucker & Schaeffel, 2004		4week		Photography from frozen	0,06 (4 week)
	Jester, 2001	8	Adult	in vivo	Confocal microscopy	0,1129 (adult)
	Schmucker & Schaeffel, 2004	3	22-100	ex vivo	Photography from frozen	0,0635 (4 week)
Posterior corneal radius	Schmucker & Schaeffel, 2004		22-100	ex vivo	Photography from frozen	1,4084 (4 week)*
n corneal	Retmulla & Hallet, 1985		20-23 weeks	ex vivo	refractometry / interferometry	1,4015 (4 week)*
Anterior chamber	Schmucker & Schaeffel, 2004		4week		OLCI	0,42 (4 week)*
	Schmucker & Schaeffel, 2004		4week		Photography from frozen	0,266 (4 week)
	Schmucker & Schaeffel, 2004	3	22-100	ex vivo	Photography from frozen	0,2012 (4 week)
n aqueous	Retmulla & Hallet, 1985		20-23 weeks	ex vivo	refractometry / interferometry	1,3336 (Adult)*
Anterior radius lens	Schmucker & Schaeffel, 2004	3	22-100	ex vivo	Photography from frozen	0,9993 (4 week)*
Lens thickness	Schmucker & Schaeffel, 2004	3	22-100	ex vivo	Photography from frozen	1,7729 (4 week)*
n lens	Schmucker & Schaeffel, 2004					1,433 (eff)
	Retmulla & Hallet, 1985		20-23 weeks	ex vivo	refractometry / interferometry	1,659 (eff)
Posterior radius lens	Schmucker & Schaeffel, 2004	3	22-100	ex vivo	Photography from frozen	1,0549 (4 week)*
n post chamb	Retmulla & Hallet, 1985		20-23 weeks	ex vivo	refractometry / interferometry	1,3329 (Adult)*
Axial length	Schmucker & Schaeffel, 2004		4week		OLCI	3,15 (4 week)*
	Schmucker & Schaeffel, 2004		4week		Photography from frozen	3,02 (4 week)
	Schmucker & Schaeffel, 2004	3	22-100	ex vivo	Photography from frozen	2,9031 (4 week)
	Tejedor & de la Villa, 2003	18	30	ex vivo	Photography from frozen	3,264 (30 day)

Table 6.2. A compilation of mice biometric data used in this work. Empty cells are data no indicated by authors.

6.3. Methods

6.3.1. Computer model for the chick eye

Computer eye models were designed in Zemax (Optima Research, Tucson, AZ), using the geometrical parameters and index of refraction of Table 6.3.

Aberrations were simulated using ray tracing in Zemax (using 150 rays across the pupil, for circular 1.5 mm-diameter pupils, and the Zernike coefficients compared to those measured experimentally. Since all surfaces were modeled as rotationally symmetric, only defocus and spherical aberration will be evaluated.

Author	Eye parameter	Age (days)		
		0	7	14
	Corneal radius (mm)	2.6670	2.7800	3.1850
Montiani-Ferrerira (2004)	Corneal thickness (mm)	0.2421	0.2394	0.2390
Choh & Sivak (2005)	n corneal	1.3730		
Schaeffel & Howland (1988,a)	Anterior Chamber Depth (mm)	1.0617	1.1266	1.2105
	n anterior chamber	1.3350		
	Anterior lens radius (mm)	2.7695	3.1000	3.4003
	Lens thickness (mm)	2.2007	2.2269	2.3000
	Posterior lens radius (mm)	1.9876	2.2651	2.5000
	n Lens periphery	1.3710	1.3722	1.3786
Sivak & Mandelmann (1982)	n Lens core	1.3947	1.3947	1.3947
	n posterior chamber	1.3352		
	Posterior chamber depth (mm)	3.6690	3.9700	5.0320

Table 6.3 Data used in chick model for days 0,7 & 14

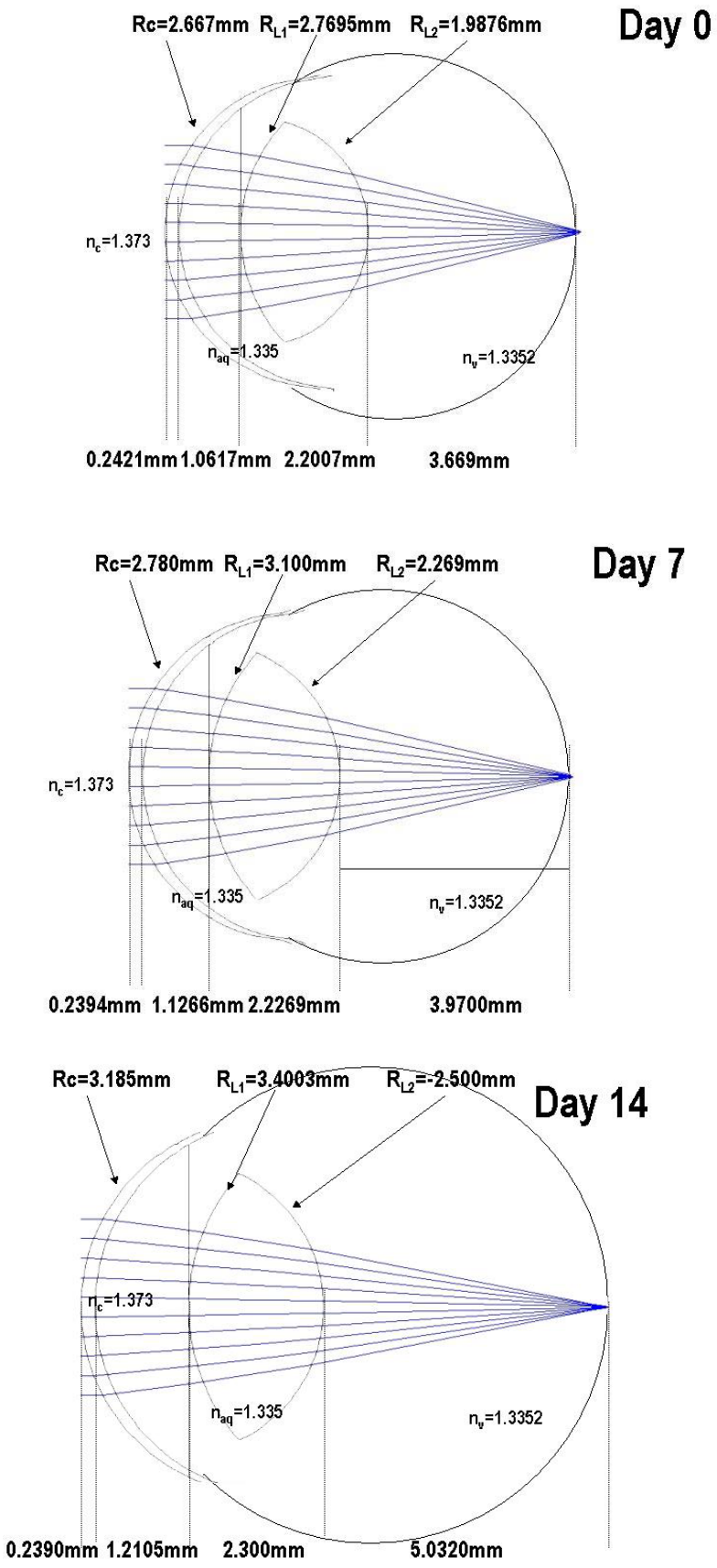

Figure 6.8 Schematic diagrams of chick eye models for days 0,7 and 14

Simulations were performed for three days during the measurement period of the experiments of Chapter 3 (0, 7 and 14days), for both normal eyes and myopia-developing eyes. Some parameters (refractive index of the cornea and humors) were kept constant with time and refractive error. Other parameters (corneal and lens radius, anterior and posterior chamber depth, lens thickness and index refractive lens) were allowed to vary with time according to the patterns described in the literature (and explained in detail in Section 6.2.1., while distribution of the index refractive lens was allowed to vary to optimize the match between simulated and measured aberrations. Simulation diagramas of chick eye for 0, 7 and 14days are in Figure 6.8.

The best fits of the model, obtained with the parameters shown in yellow circle symbols in Figures 6.1-6.7., will be shown in graphical form as a function of age in comparison with linear fits of the experimental values of defocus and spherical aberration from Chapter 3.

6.3.2. Computer model for the mouse eye

Using similar procedures as those described for the chick eye, we simulated the mouse model eye in Zemax, and the spherical error and spherical

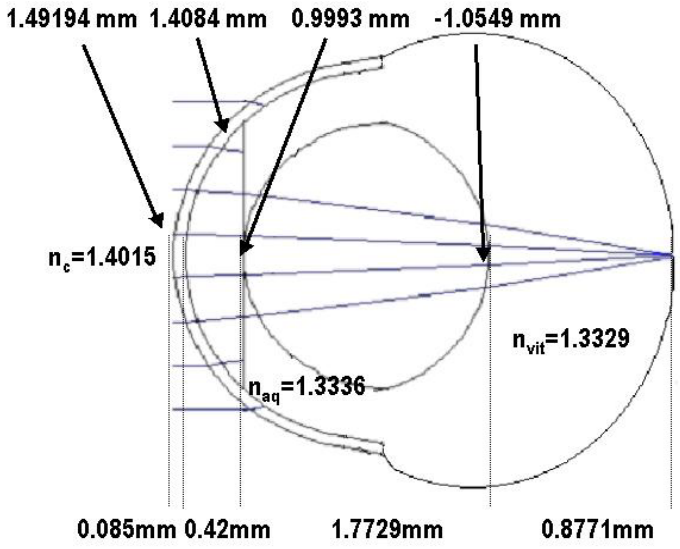

Figure 6.9 4-week old mouse schematic eye. Axial dimensions, radii and refractive indices are shown.

aberration were simulated using ray tracing. Figure 6.9 shows the mouse schematic eye (wild-type, 4-week old). The only variable in this model was the lens refractive index distribution.

6.4. Results

6.4.1. Chick eye model

Figure 6.10 shows simulated defocus (from Z_{20} Zernike term) for days 0, 7 and 14 and a linear regression to the retinoscopy experimental data of Chapter 3 for emmetropic eye (A) and axial elongated myopic eye (B).

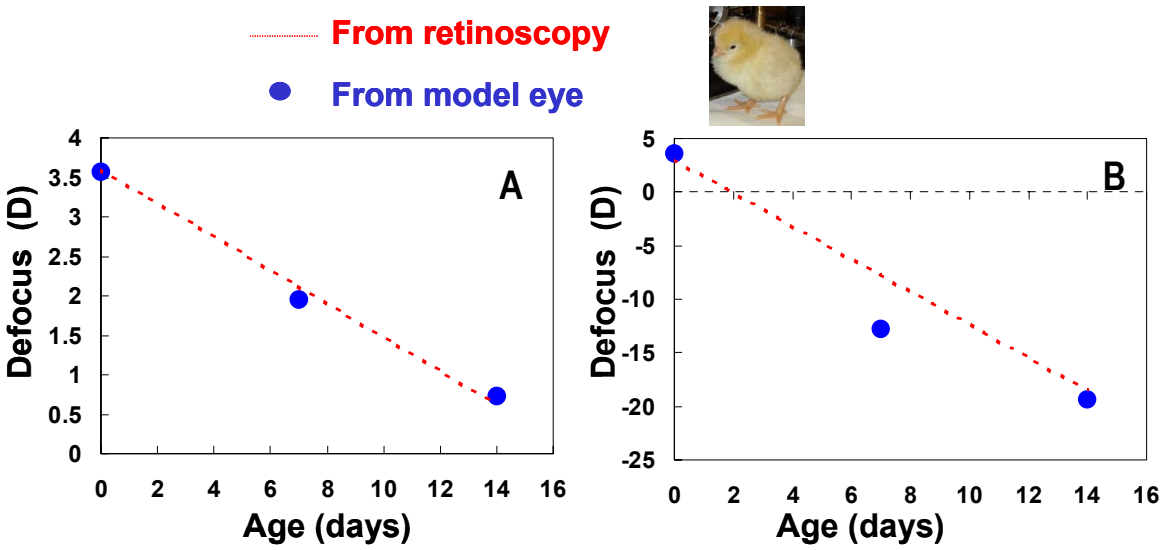

Figure 6.10 Longitudinal values of defocus obtained form Z_{20} Zernike coefficients from retinoscopy (see Chapter 3) and computer eye model for the chick eye: (A) Emmetropic eye (B) Myopic eye where only axial elongation has been modified.

Figure 6.11 shows simulated spherical aberration (from Z40) for days 0, 7 and 14 and a linear regression to the Hartmann-Shack experimental spherical aberration of Chapter 3 for emmetropic eye (A) and axial elongated myopic eye (B).

We have found that the model predicts accurately the amounts of refractive error, and the rate of change of refractive error in normal and form-deprived chick eyes. Most interestingly, the model is able to predict the

decrease of spherical aberration with age in normal eyes, and the increase of spherical aberration in emmetropic eyes. While the trends are well reproduced, the model fails at reproducing the exact amounts of spherical aberration (although it should be noted that in all cases the values are very small, and trends seem more important than the actual amount).

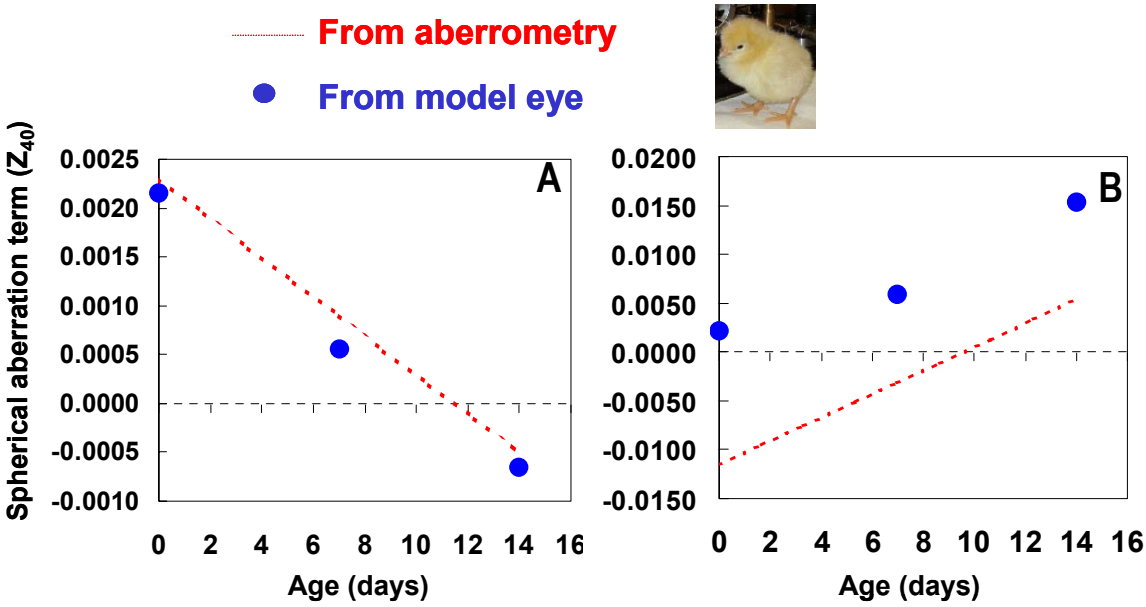

Figure 6.11 Spherical aberration term (Z_{40} Zernike coefficient) from aberrometry (see Chapter 3) and computer eye model for the chick eye: (A) Emmetropic eye (B) Myopic eye where only axial elongation has been modified.

We found that the best fits (simultaneously for defocus and spherical aberration) and trends were obtained when the only different parameter between emmetropic and myopic chick eyes is axial length. The use of steeper corneal radii of curvature in myopic chicks (Gottlieb et al. 1987; Schaeffel and Howland 1988; Irving et al. 1992) resulted in excessive myopia (for the axial lengths under consideration), and larger amounts of spherical aberration than those observed experimentally. The same effect has an increase of the anterior chamber depth.

Also, we found that the best simultaneous fits were obtained using a gradient index profile for the lens. When a homogeneous lens refractive index is kept constant with increasing age (for example, the effective index reported by Schaeffel & Howland (1988) 1.455), refractive error tends toward hyperopia in

the normal eye from -3.351 microns in day o to -8.6 microns in day 14, and the ocular spherical aberration tends toward more negative values (from Z40= +1.17 microns to Z40= -0.08microns). To account for the measured changes in defocus, the effective index of the lens each should increase with age from 1.467 to 1.518 between day 0 and 14. In this chick model with a homogeneous lens the spherical aberration in the normal eye decreased from 1.17 microns (3.6 D) to 0.034 microns (0.5 D). In myopic eyes when effective index (1.455) is constant with age the experimental rate of increase of myopia is not well reproduced, and the spherical aberration decreases.

The gradient index distribution that best reproduces the experimental data consists of a constant value in lens core (1.3947), and an age-dependent index in the periphery of the lens (day 0: 1.3710; day 7: 1.3722; day 14: 1.3786). This is also anatomically plausible, consistent with lens fibers growing from the center to the cortex

These results indicate that changes in the refractive lens are essential to account for fine tuning of axial length to optical power, and that a gradient index profile would account for the fine tuning of the spherical aberration and its disrupture in myopia development.

In human eyes, the asphericity of the cornea, and presumably the asphericity of the lens plays a major role in determining the total spherical aberration of the eye (to the extent that newer generations of intraocular lenses are designed with aspherical surfaces so that they produce negative spherical aberration to compensate the spherical aberration of the cornea (Marcos et al. 2005). We modeled corneal asphericity, according to, to our knowledge, the only value reported in the literature on a single chick.

When the corneal asphericity reported by Schaeffel & Howland (1988) (-1.12) is considered, a larger hyperopic values and more negative spherical aberration is obtained. In general, we were not able to reproduce refractive and spherical aberration trends with aging and refractive error only adjusting surface asphericities.

In summary, the most plausible model, in accordance to most reported anatomical parameters and observations, differences in elongation can explain the differences in the change rate of both refraction and spherical aberration between normal and myopia-developing form-deprived eye. Other structural differences appear to have minor contribution. A gradient index model is needed to explain the low amounts of spherical aberration present (both the fine-tuning in emmetropic eyes and the slight increase with age in myopic eyes).

6.4.2. Mouse eye model

Defocus and spherical aberration have been simulated using Ray tracing in Zemax on the schematic model of Fig. 6.8. A comparison of a aberration map obtained form Zernike coefficients of the computer model and from aberrometry in a real mouse are plotted in Figure 6.12.The best fit to the experimental data of refraction and spherical aberration have been obtained using a spherical gradient index model in the crystalline lens, with n=1.4295 and 1.373 in the core and the periphery, and α=-0.12747476, β=-0.07190183 in equation 6.1 With these data Z_{20}=-0.82 microns (average experimental Z_{20}=-0.81 microns –or +2.48 D- and Z_{40}=0.14 microns (average experimental Z_{40}=0.1445). For a homogeneous lens, we computed that for an effective index of 1.44465, the defocus term is well reproduced (Z_{20}=-0.8 microns), but the simulated spherical aberration (Z_{40}=5.2 microns) is 5.06 microns, much higher than the experimental value.

As a centered, rotationally symmetric model has been assumed, and no attempt has been made to reproduce the relatively high amounts of coma found experimentally in Chapter 5. A further refinement of the model incorporates biconic surfaces (ellipse), where the radius is modified toward periphery, we found that a conic constant k_x=-0.005 reproduced the astigmatism data measured in 4-week old chicks (Z_{2-2}=-0.12microns).

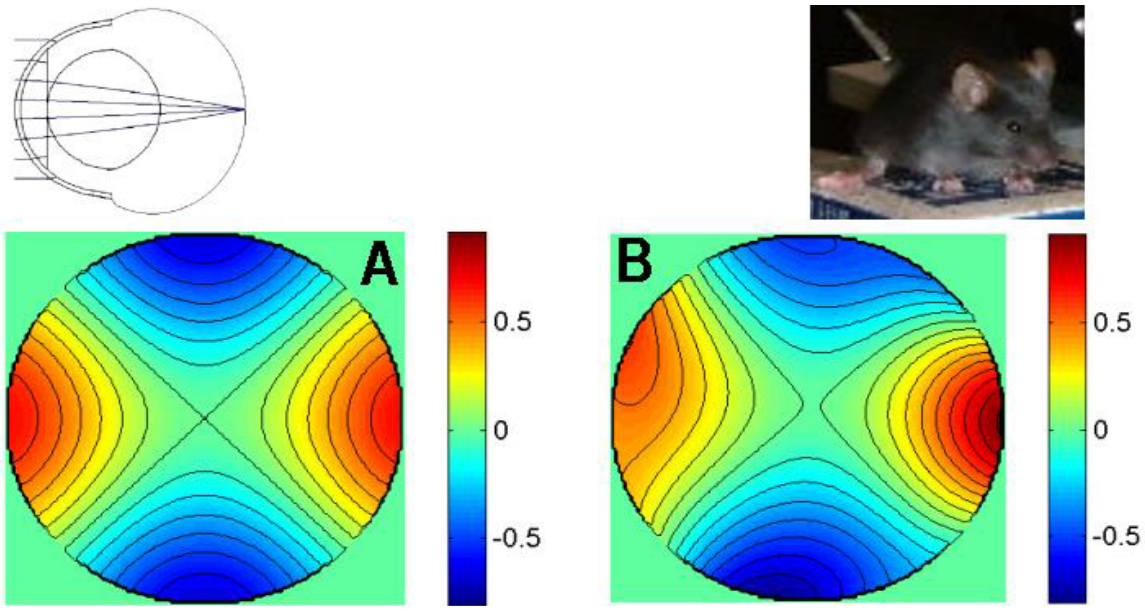

Figure 6.12 Aberration maps for a 4-week old mouse (A) Hartmann-Shack experimental measurement. (B) simulated by ray tracing on a model eye (with a biconic corneal surface).

6.5. Discussion

6.5.1. Chick eye model

We have shown that an eye model with geometrically consistent with the literature is able to reproduce: 1) the shift toward emetropia from 0-14 days in normal chick eyes, and the rate of myopia development in form-deprived eyes. 2) the decrease of spherical aberration from day 0, and relative low values of spherical aberration in both normal and form-deprived myopic chick eyes. 3) the slightly higher amounts of spherical aberration in myopic chick eyes. We found that the differences between emmetropic and myopic eyes are primarily explained by differences in the posterior chamber depth. We also found that a gradient index distribution in the crystalline lens (a simple parabolic model, consistent with measurements of the index of refraction at the lens core and surface) was necessary to explain the low amounts of spherical aberration found in chick eyes.

Previous computer eye models (with cornea and crystalline lens) aimed primarily at predictions of the refractive state. In most cases an effective index of refraction is used in the lens, rather than a gradient index distribution. A

model using an onion-like structure in the crystalline lens had been previously used to explain spherical aberration in a 30-day old chick eye, but accuracies higher than 0.5 D and explanation of longitudinal changes were not attempted (Schaeffel and Howland 1988).

Previous attempts to explain higher order aberrations, and particularly their relative change with development (i.e. increasing size of the globe) were based on very simple models, namely with only one surface and functional expressions for eye growth. Howland (Howland 2005) proposed that for a growing eye with an increase factor of k, the RMS for a constant pupil size, should decrease by a factor of $1/k^{n-1}$, with n=3.9 and k a 2^{nd} order polynomial of age as reported by Mihashi et al 2004 (Mihashi et al. 2004). Despite its simplicity, this model is able to predict surprisingly well the general trend of our experimental data (decrease of high order aberrations for a constant pupil size), but it fails at reproducing the actual amounts of aberrations, and at capturing the differences between myopic and emmetropic eyes (i.e. the fact that axial elongation can be associated to larger amounts of spherical aberration).

While our model represents a significant sophistication over existing chick model eyes, the fact that the model is based on rotationally symmetric surfaces prevents it from reproducing the significant amounts of coma and other high order asymmetric aberrations found in the chick eye, which may arise from corneal irregularities and ocular surface misalignments. Also, as any other schematic model, it is only able to capture average trends and magnitudes, and not individual differences which were significant in experimentally measured aberrations.

6.5.2. Mouse eye model

We found that a model using reported biometric data and spherical gradient index model is able to capture the refractive state and amount of spherical aberration in a 4-week old wild type mouse. A gradient index distribution in the lens was necessary to account for the lower values of

spherical aberration (compared to a homogeneous lens), although the indices in the lens core and periphery were lower than those reported by Hughes (Hughes 1979) (1.5 and 1.39 respectively) in the adult rat, as these values resulted in high amounts of myopia when used in the mouse. The equivalent effective index that reproduced accurately the measured refractive error (assuming the geometrical parameters of Fig. 6.9) was 1.44465, much similar to that proposed by Schmucker and Schaeffel 2004a) (Schmucker and Schaeffel 2004), 1.433, than that reported by Retmulla & Hallet (Remtulla and Hallett 1985) 1.659, which would result in high amounts of myopia.

Artal et al.(Artal et al. 1998) developed an optical model of the rat eye. They found that in a small eye, the steeper surfaces result in high amount of aberrations, but the corresponding simulated MTFs were still higher than the experimental double-pass MTFs. This is in contrast to our finding, that, despite the highly degraded optics in the mouse, there seems to be still some compensation (most likely in the form of gradient index distribution in the lens) that prevents for even higher amounts of spherical aberration predicted from geometry (and constant index). The higher optical degradation found in double-pass experiments (higher than from Hartmann-Shack measurements and from computer eye model simulations) could have arisen from intraocular or retinal scattering.